Modeling of passively *Q*-switched lasers

Xingyu Zhang, Shengzhi Zhao, and Qingpu Wang

Department of Optics, Shandong University, Jinan 250100, China

B. Ozygus and H. Weber

Optical Institute, TU-Berlin, Strasse des 17 Juni 135, D-10623 Berlin, Germany

Received October 18, 1999; revised manuscript received March 20, 2000

The intracavity photon density and the initial population-inversion density in the diode-pumped passively *Q*-switched laser rate equations are assumed to be Gaussian spatial distributions. These space-dependent rate equations are solved numerically, and a group of general curves are generated. These curves clearly show the dependence of the pulse characteristics on the pump- to laser-mode size ratio and the parameters of the gain medium, the saturable absorber, and the resonator. They can also be used to estimate the pulse parameters of an arbitrary diode-pumped passively *Q*-switched laser and to determine the optimal pump- to laser-mode size ratio. In addition, these curves are not limited to diode-pumped lasers. Sample calculations for a diode-pumped Nd^{3+}:YVO_4 laser and a flash-lamp pumped Nd^{3+}:YAG laser are presented to demonstrate the use of the curves and the related formulas. © 2000 Optical Society of America [S0740-3224(00)00807-9]

OCIS codes: 140.3430, 140.3460, 140.3480, 140.3540, 140.3580.

1. INTRODUCTION

Pulses in the nanosecond and subnanosecond regimes with high peak power and high repetition rate have wide applications in nonlinear optics, spectroscopy, ranging, and remote sensing. Laser-diode (LD) pumped passively *Q*-switched lasers can generate this kind of pulse and have the advantages of simplicity, compactness, low cost, and high efficiency. Therefore LD-pumped passively *Q*-switched lasers have attracted a great deal of attention in recent years.[1–6]

The standard tools for analyzing the performance of a *Q*-switched laser are the rate equations. Szabo *et al.* first derived the relevant rate equations for the passively *Q*-switched lasers and presented some numerical results.[7,8] These rate equations have been widely referred to and appropriately modified.[9–12] For lasers passively *Q*-switched by slow saturable absorbers with excited-state absorption, the analytical solutions of the equations have also been obtained.[13] However, the above-mentioned rate equations are obtained under the plane-wave approximation, in which the assumption of uniform pumping, uniform intracavity laser intensity, and uniform bleaching of the saturable absorber has been made. For an LD-pumped passively *Q*-switched laser, this assumption is not properly satisfied. Besides, the spatial variation of pumping and intracavity intensity in the rate equations of an LD-pumped cw laser has been considered,[14–18] and the importance of including the spatial variation has been shown.[14] Recently, the LD-pumped actively *Q*-switched lasers have been modeled by the assumption that the intracavity photon density and the initial population-inversion density in the rate equations are Gaussian spatial distributions, and the importance to do this has also been shown.[19] For a more accurate theoretical analysis of the *Q*-switched laser pulses, particularly of the influence of the pump- and laser-mode sizes on the laser characteristics, it is desirable to consider the spatial variations of the intracavity photon density, the population-inversion density of the gain medium, and the ground-state population density of the saturable absorber in the rate equations of LD-pumped passively *Q*-switched lasers.

In this paper the intracavity photon density is assumed to be a Gaussian spatial distribution during the entire formatting process of the LD-pumped passively *Q*-switched laser pulse, the population-inversion density at $t = 0$ is also assumed to be a Gaussian spatial distribution, and the ground-state population density of the saturable absorber at $t = 0$ is assumed to be uniform. These space-dependent rate equations are solved numerically, and a group of general curves are generated. These curves can give us a good understanding of the dependence of the laser-pulse characteristics on the parameters about the pumping, the gain medium, the saturable absorber, and the resonator. From these curves and the related formulas, pulse energy, peak power, pulse width, and laser efficiency can be easily estimated, and the optimal pump- to laser-mode size ratio can be determined. In addition, these curves and the related formulas are not limited to LD-pumped passively *Q*-switched lasers. The parameters of an LD-pumped Cr^{4+}:YAG passively *Q*-switched Nd^{3+}:YVO_4 laser and a flash-lamp-pumped Cr^{4+}:YAG passively *Q*-switched Nd^{3+}:YAG laser are calculated as examples to demonstrate the use of the curves and the related formulas.

2. RATE EQUATIONS

The intracavity photon density $\phi(r, t)$ for the TEM_{00} mode can be expressed as

$$\phi(r, t) = \phi(0, t)\exp\left(-\frac{2r^2}{\omega_L^2}\right), \tag{1}$$

 © 2000 Optical Society of America

where r is the radial coordinate, ω_L is the laser-mode radius, which is mainly determined by the geometry of the resonator, and $\phi(0,t)$ is the photon density in the laser axis.

In the rate equations of a passively Q-switched laser, the spatial variations of the population-inversion density of the gain medium and the ground-state population density of the saturable absorber should also be considered. Besides, the differential equation describing $\mathrm{d}\phi(r,\, t)/\mathrm{d}t$ should be integrated over the beam cross section to guarantee the beam Gaussian spatial distribution during the entire formatting process of the Q-switched pulse. By making the above modifications to the rate equations in Ref. 13 and considering the difference between the beam cross-section areas in the gain medium and in the saturable absorber, we obtain

$$\int_0^\infty \frac{\mathrm{d}\phi(r,\, t)}{\mathrm{d}t} 2\pi r \mathrm{d}r = \int_0^\infty \frac{\phi(r,\, t)}{t_r} \{2\sigma n(r,\, t) l - 2\sigma_{\mathrm{gsa}} n_{\mathrm{sg}}(r,\, t) l_s - 2\sigma_{\mathrm{esa}}[n_{s0} - n_{\mathrm{sg}}(r,\, t)] l_s - \ln(1/R) - L\} 2\pi r \mathrm{d}r, \tag{2}$$

$$\frac{\mathrm{d}n(r,\, t)}{\mathrm{d}t} = -\gamma\sigma c\, \phi(r,\, t) n(r,\, t), \tag{3}$$

$$\frac{\mathrm{d}n_{\mathrm{sg}}(r,\, t)}{\mathrm{d}t} = -\frac{S_g}{S_s} \sigma_{\mathrm{gsa}} c\, \phi(r,\, t) n_{\mathrm{sg}}(r,\, t), \tag{4}$$

where $n(r,\, t)$ is the population-inversion density; $n_{\mathrm{sg}}(r,\, t)$ and n_{s0} are, respectively, the ground-state and total population densities of the saturable absorber; σ and l are, respectively, the stimulated-emission cross section and length of the gain medium; σ_{gsa} and σ_{asa} are, respectively, the ground-state and excited-state absorption cross sections of the saturable absorber; l_s is the length of the saturable absorber; $t_r = 2l'/c$ is the round-trip transit time of light in the resonator of optical length l', c is the light speed in vacuum, R is the reflectivity of the output mirror, L is the remaining round-trip dissipative optical loss; S_g and S_s are, respectively, the beam cross-section areas in the gain medium and in the saturable absorber; and γ is the inversion-reduction factor, which actually corresponds to the net reduction in the population inversion resulting from the stimulated emission of a single photon. In Eqs. (2)–(4) the pumping and the spontaneous emission during the pulse formation are neglected. Since most solid-state saturable absorbers are of slow recovery (i.e., the passively Q-switched pulse duration is much shorter than the first excited-state lifetime of the saturable absorber[10,20–23]), the ground-state recovery of the saturable absorber during the formation of the Q-switched pulse is also neglected.

For end-pumped lasers, since the pump-light intensity in the gain medium is attenuated along the longitudinal axis z, $n(r,\, t)$ is also a function of z. In this paper we focus on the influence of the pump- and laser-mode sizes on the passively Q-switched pulse characteristics. $n(r,\, t)$ in the above equations represents average value, i.e., $n(r,\, t) = \int_0^l n(r,\, z,\, t)\mathrm{d}z/l$. For side-pumped lasers it is reasonable to consider $n(r,\, t)$ to be independent of z.

The initial photon density $\phi(r,\, 0)$ should be zero. When the rate equations are solved numerically, $\phi(r,\, 0)$ can be set at a value much smaller than the peak value of the photon density $\phi_m(r,\, t)$ [for example, $\phi(r,\, 0) = 10^{-4}\phi_m(r,\, t)$]. If $\phi(r,\, 0)$ is even smaller, the pulse buildup time will become longer, but the pulse energy and pulse width are not changed. The initial value of $n_{\mathrm{sg}}(r,\, t)$ can be considered to be n_{s0}. This is because the ground-state recovery times of the saturable absorbers are much shorter than the time interval between two successive pulses; before a Q-switched pulse is generated, the saturable absorber can completely recover from its bleached status caused by the preceding Q-switched pulse. The initial population-inversion density $n(r,\, 0)$ can be assumed to be a Gaussian spatial distribution.[19] Thus the initial conditions of Eqs. (2)–(4) can be written as

$$\phi(r,\, 0) \approx 10^{-4}\phi_m(r,\, t), \tag{5}$$

$$n_{\mathrm{sg}}(r,\, 0) = n_{s0}, \tag{6}$$

$$n(r,\, 0) = n(0,0)\exp\left(-\frac{2r^2}{\omega_p^2}\right), \tag{7}$$

where ω_p is the average radius of the pump beam in the gain medium, and $n(0,0)$ is the initial population-inversion density in the laser axis. For side-pumped lasers it is reasonable to consider $n(r,\, 0)$ to be uniform, which corresponds to the case of a Gaussian spatial distribution when $\omega_p \to \infty$. We can estimate $\phi_m(r,\, t)$ in formula (5) by consulting the results obtained under the plane-wave approximation or by preliminarily solving the equations.

Substituting Eqs. (1), (6), and (7) into Eqs. (3) and (4) and integrating the results over time, we obtain

$$n(r,\, t) = n(0,0)\exp\left(-\frac{2r^2}{\omega_p^2}\right) \times \exp\left[-\gamma\sigma c \exp\left(-\frac{2r^2}{\omega_L^2}\right)\int_0^t \phi(0,t)\mathrm{d}t\right], \tag{8}$$

$$n_{\mathrm{sg}}(r,\, t) = n_{s0}\exp\left[-\frac{S_g}{S_s}\sigma_{\mathrm{gsa}} c \times \exp\left(-\frac{2r^2}{\omega_L^2}\right)\int_0^t \phi(0,t)\mathrm{d}t\right]. \tag{9}$$

Substituting Eqs. (1), (8), and (9) into Eq. (2) and regrouping the result yields

$$\frac{\mathrm{d}\phi(0,t)}{\mathrm{d}t} = \frac{4\sigma n(0,0)l\,\phi(0,t)}{\omega_L^2 t_r} \times \int_0^\infty \exp\left[-\gamma\sigma c\exp\left(-\frac{2r^2}{\omega_L^2}\right)\int_0^t \phi(0,t)\mathrm{d}t\right] \times \exp\left[-2r^2\left(\frac{1}{\omega_p^2}+\frac{1}{\omega_L^2}\right)\right]2r\mathrm{d}r - \frac{4(\sigma_{\mathrm{gsa}}-\sigma_{\mathrm{esa}})n_{s0}l_s\phi(0,t)}{\omega_L^2 t_r} \times \int_0^\infty \exp\left[-\frac{S_g}{S_s}\sigma_{\mathrm{gsa}}c\exp\left(-\frac{2r^2}{\omega_L^2}\right)\int_0^t\phi(0,t)\mathrm{d}t\right] \times \exp\left(-\frac{2r^2}{\omega_L^2}\right)2r\mathrm{d}r - \frac{\phi(0,t)}{t_r} \times \left[\ln\left(\frac{1}{R}\right)+\left(\frac{\sigma_{\mathrm{esa}}}{\sigma_{\mathrm{gsa}}}\right)\ln\left(\frac{1}{T_0^2}\right)+L\right], \tag{10}$$

where T_0 is the small-signal transmission of the saturable absorber, i.e.,

$$T_0 = \exp(-\sigma_{\mathrm{gsa}}n_{s0}l_s). \tag{11}$$

Equation (10) is the basic differential equation describing $\phi(0,t)$ as a function of t.

3. SOLUTIONS OF THE RATE EQUATIONS

Since laser action begins at the moment that the population-inversion density crosses the initial threshold value in a passively Q-switched laser, by setting Eq. (10) equal to zero and $t = 0$ and using Eq. (11), we obtain the initial population-inversion density in the laser axis:

$$n(0,0) = \frac{\ln\left(\frac{1}{R}\right)+\ln\left(\frac{1}{T_0^2}\right)+L}{2\sigma l}\left(1+\frac{\omega_L^2}{\omega_p^2}\right). \tag{12}$$

We introduce the normalized time τ and normalized photon density $\Phi(r,\ \tau)$ and define a new parameter N:

$$\tau = \frac{t}{t_r}\left[\ln\left(\frac{1}{R}\right)+\ln\left(\frac{1}{T_0^2}\right)+L\right], \tag{13}$$

$$\Phi(r,\ \tau) = \phi(r,\ \tau)\frac{2\gamma\sigma l'}{\ln\left(\frac{1}{R}\right)+\ln\left(\frac{1}{T_0^2}\right)+L}, \tag{14}$$

$$N = \frac{\ln\left(\frac{1}{R}\right)+\ln\left(\frac{1}{T_0^2}\right)+L}{\ln\left(\frac{1}{R}\right)+\left(\frac{\sigma_{esa}}{\sigma_{\mathrm{gsa}}}\right)\ln\left(\frac{1}{T_0^2}\right)+L}. \tag{15}$$

Substituting Eqs. (13), (14), and (15) into Eq. (10) and regrouping the result, we obtain

$$\frac{\mathrm{d}\Phi(0,\tau)}{\mathrm{d}\tau} = \Phi(0,\tau)\int_0^1 \exp\{-A(\tau)y^\beta\}\mathrm{d}y - \left(1-\frac{1}{N}\right)\Phi(0,\tau)\frac{1-\exp[-\alpha A(\tau)]}{\alpha A(\tau)} - \frac{\Phi(0,\tau)}{N}, \tag{16}$$

where

$$y = \exp\left[-2r^2\left(\frac{1}{\omega_L^2}+\frac{1}{\omega_p^2}\right)\right], \tag{17}$$

$$\beta = \frac{1}{1+(\omega_L/\omega_p)^2}, \tag{18}$$

$$A(\tau) = \int_0^\tau \Phi(0,\tau)\mathrm{d}\tau, \tag{19}$$

$$\alpha = \frac{\sigma_{\mathrm{gsa}}S_g}{\gamma\sigma S_s}. \tag{20}$$

Equation (16) is just the differential equation describing the normalized photon density in the laser axis versus the normalized time. The solutions of Eq. (16) are dependent on three synthetic parameters: α, N, and ω_p/ω_L.

α is a mark indicating how easily the saturable absorber is bleached. The larger α is, the more easily the saturable absorber is bleached.[11,13]

When α approaches infinity, once the laser action begins, all the ground-state population will be excited to the first excited state [which we can see from Eq. (9) by setting $\sigma_{\mathrm{gsa}} \to \infty$, which corresponds to $\alpha \to \infty$]. Owing to the excited-state absorption, the transmission of the saturable absorber will be

$$T_b = \exp(-\sigma_{\mathrm{esa}}n_{s0}l_s) = T_0^{(\sigma_{\mathrm{esa}}/\sigma_{\mathrm{gsa}})}, \tag{21}$$

and the threshold population-inversion density in the laser axis will be

$$n_{\mathrm{th}}(0,t) = \frac{\ln\left(\frac{1}{R}\right)+\left(\frac{\sigma_{\mathrm{esa}}}{\sigma_{\mathrm{gsa}}}\right)\ln\left(\frac{1}{T_0^2}\right)+L}{2\sigma l}\left(1+\frac{\omega_L^2}{\omega_p^2}\right). \tag{22}$$

From Eqs. (12), (15), and (22) it can be seen that N is the ratio of the initial population-inversion density to the threshold population-inversion density in the case of $\alpha \to \infty$. N has a physical meaning similar to n_i/n_{t0} under the plane-wave approximation in Ref. 13. n_i/n_{t0} is also the ratio of the initial population-inversion density to the threshold population-inversion density in the case of $\alpha \to \infty$ under the plane-wave approximation. N and n_i/n_{t0} are all determined by the parameters of the saturable absorber and resonator, and they have the same expression.[13]

ω_p/ω_L is a unique parameter when the spatial variation of the pumping and intracavity laser intensity is considered. The dependence of the pulse parameters on ω_p/ω_L is a major part of this paper.

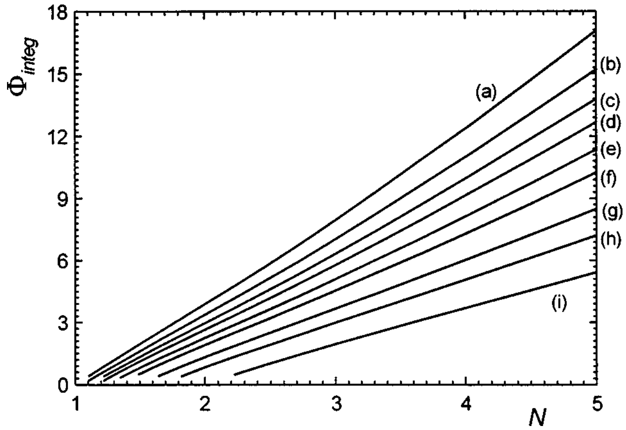

Fig. 1. Relation between Φ_{integ} and N for different α in the case of $\omega_p \gg \omega_L$. Φ_{integ} is the integral of $\Phi(0, \tau)$ over τ from zero to infinity as shown in Eq. (26); N is determined by Eq. (15): (a) $\alpha \to \infty$, (b) $\alpha = 20$, (c) $\alpha = 10$, (d) $\alpha = 7$, (e) $\alpha = 5$, (f) $\alpha = 4$, (g) $\alpha = 3$, (h) $\alpha = 2.5$, (i) $\alpha = 2$.

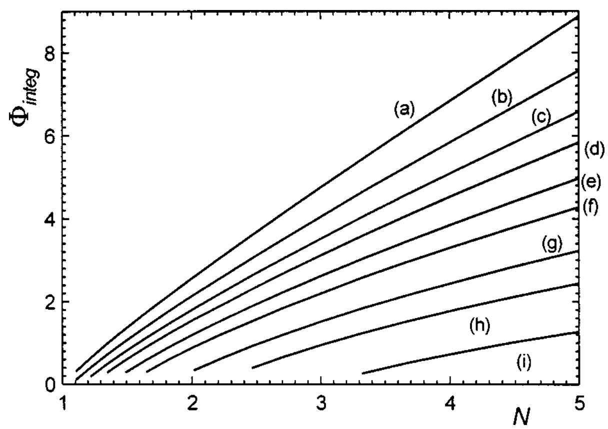

Fig. 2. Same as Fig. 1 except for $\omega_p = \omega_L$.

By numerically solving Eq. (16), we can obtain $\Phi(0, \tau)$ for different N, different α, and different ω_p/ω_L. From the shape of $\Phi(0, \tau)$ we can obtain the normalized pulse duration $\Delta\tau$. The real pulse width W is

$$W = \frac{\Delta\tau t_r}{\ln\left(\frac{1}{R}\right) + \ln\left(\frac{1}{T_0^2}\right) + L}. \tag{23}$$

By using the method of Ref. 24, we can obtain the following expressions for pulse peak power P_m and pulse energy E:

$$P_m = \frac{\pi\omega_L^2 h\nu}{4\sigma\gamma t_r}\left[\ln\left(\frac{1}{R}\right) + \ln\left(\frac{1}{T_0^2}\right) + L\right]\ln\left(\frac{1}{R}\right)\Phi_m, \tag{24}$$

$$E = \frac{\pi\omega_L^2 h\nu}{4\sigma\gamma}\ln\left(\frac{1}{R}\right)\Phi_{\mathrm{integ}}, \tag{25}$$

where $h\nu$ is the photon energy, Φ_m is the maximum value of $\Phi(0, \tau)$, and Φ_{integ} is the integral of $\Phi(0, \tau)$ over τ from zero to infinity, i.e.,

$$\Phi_{\mathrm{integ}} = \int_0^\infty \Phi(0, \tau)\mathrm{d}\tau. \tag{26}$$

Figures 1–3 show the variation of Φ_{integ} with N for different α in the cases of $\omega_p \gg \omega_L$, $\omega_p = \omega_L$, and $\omega_p \ll \omega_L$, respectively. Figures 4–6 show the variation of Φ_{integ} with ω_p/ω_L for different α in the cases of $N = 4$, 3, and 2, respectively. In each of Figs. 1–6, values of α are (a) $\alpha \to \infty$, (b) $\alpha = 20$, (c) $\alpha = 10$, (d) $\alpha = 7$, (e) $\alpha = 5$, (f)

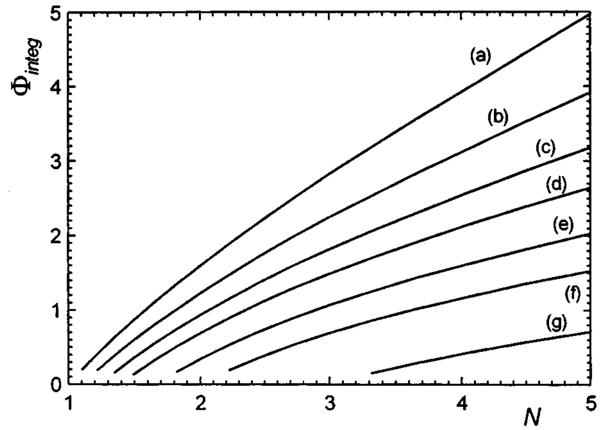

Fig. 3. Same as Fig. 1 except for $\omega_p \ll \omega_L$. Since the Q-switching cannot be realized for $\alpha = 2.5$ and $\alpha = 2$ in the case of both $\omega_p \ll \omega_L$ and $N < 5$, there are no curves (h) and (i) in this figure.

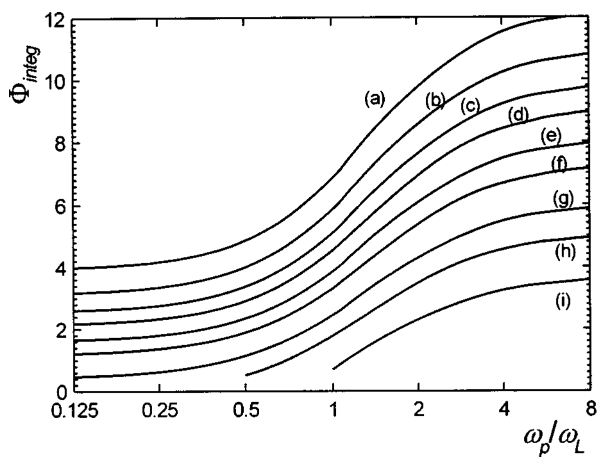

Fig. 4. Relation between Φ_{integ} and ω_p/ω_L for different α in the case of $N = 4$: (a) $\alpha \to \infty$, (b) $\alpha = 20$, (c) $\alpha = 10$, (d) $\alpha = 7$, (e) $\alpha = 5$, (f) $\alpha = 4$, (g) $\alpha = 3$, (h) $\alpha = 2.5$, and (i) $\alpha = 2$.

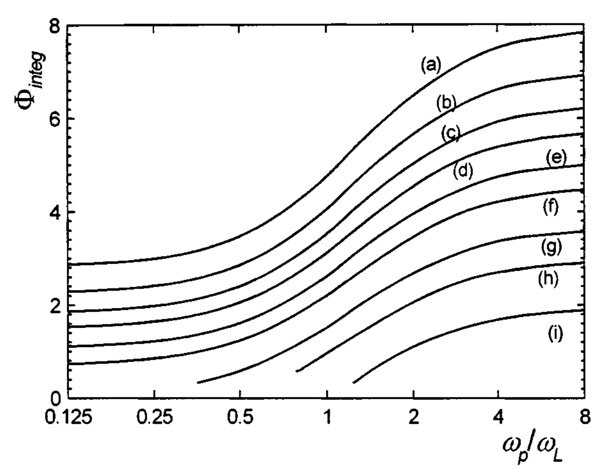

Fig. 5. Same as Fig. 4 except for $N = 3$.

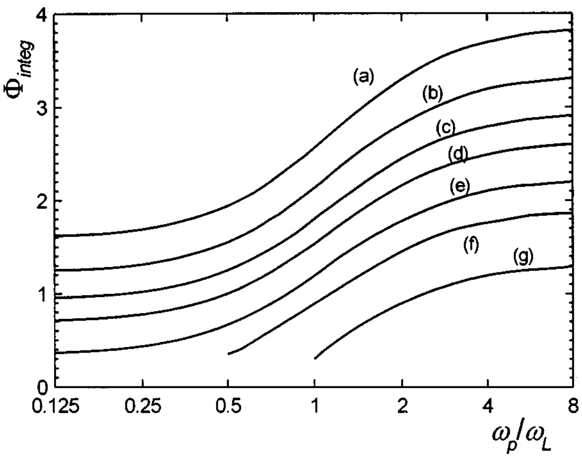

Fig. 6. Same as Fig. 4 except for $N = 2$. Since the Q-switching cannot be realized for $\alpha = 2.5$ and $\alpha = 2$ in the case of both $N = 2$ and $\omega_p/\omega_L < 8$, there are no curves (h) and (i) in this figure.

$\alpha = 4$, (g) $\alpha = 3$, (h) $\alpha = 2.5$, and (i) $\alpha = 2$. Since the Q-switching cannot be realized for $\alpha = 2.5$ and $\alpha = 2$ in the case of both $\omega_p \ll \omega_L$ and $N < 5$ or in the case of both $N = 2$ and $\omega_p/\omega_L < 8$, there are no curves (h) and (i) in Figs. 3 and 6.

From Figs. 1–3 it can be seen that Φ_{integ} increases monotonically with increasing N and α for a given ω_p/ω_L. These results are similar to those obtained under the plane-wave approximation.[13] The relation between Φ_{integ} and ω_p/ω_L deserves more comment. As can be seen from Figs. 4–6, Φ_{integ} increases monotonically with increasing ω_p/ω_L for given N and α. The slopes of the curves describing the relation between Φ_{integ} and $\log_2(\omega_p/\omega_L)$ reach their respective maximum values when ω_p/ω_L equals 1. When ω_p/ω_L is far from 1, the curves tend to be gentle. This phenomenon can be understood as follows. Since the laser mode is a Gaussian spatial distribution, the central part of the laser mode strongly interacts with the inversion population, while the peripheral part of the laser mode weakly interacts with the inversion population. If ω_p/ω_L is relatively large (for example, $\omega_p/\omega_L > 1$), when the central part of the inversion population is depleted, there is still some inversion population in the peripheral part, and it continues to interact with the laser mode. Thus a pulse with larger energy is generated. If ω_p/ω_L is relatively small, on the contrary, there is no peripheral part of the inversion population to interact with the laser mode. Thus the pulse energy is also relatively small. When ω_p/ω_L is too large (for example, $\omega_p/\omega_L > 4$), the interaction between the laser mode and the inversion population in the region $r > 4\omega_L$ is too weak. That is to say, the inversion population in the region $r > 4\omega_L$ nearly makes no contribution to the pulse energy. Therefore when $\omega_p/\omega_L > 4$, Φ_{integ} nearly keeps unchanged. When $\omega_p/\omega_L < 0.25$, almost all the inversion population can participate in the interaction with the laser mode, and the initial inversion population [the initial inversion population is the product of the initial population-inversion density shown in Eq. (12) and $\pi\omega_p^2 l/2$] nearly keeps unchanged. Therefore when $\omega_p/\omega_L < 0.25$, Φ_{integ} also nearly keeps unchanged.

Figures 7–9 show the variation of Φ_m with N for different α in the cases of $\omega_p \gg \omega_L$, $\omega_p = \omega_L$, and $\omega_p \ll \omega_L$, respectively. Figures 10–12 show the variation of Φ_m with ω_p/ω_L for different α in the cases of $N = 4$, 3, and 2, respectively. The variation tendency of Φ_m with α, N, and ω_p/ω_L is similar to that of Φ_{integ}.

Figures 13–15 show the variation of $\Delta\tau$ with N for different α in the cases of $\omega_p \gg \omega_L$, $\omega_p = \omega_L$, and ω_p

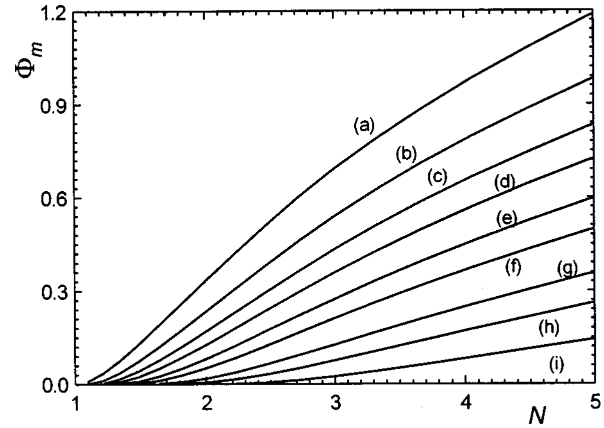

Fig. 7. Relation between Φ_m and N for different α in the case of $\omega_p \gg \omega_L$; Φ_m is the peak value of $\Phi(0, \tau)$: (a) $\alpha \to \infty$, (b) $\alpha = 20$, (c) $\alpha = 10$, (d) $\alpha = 7$, (e) $\alpha = 5$, (f) $\alpha = 4$, (g) $\alpha = 3$, (h) $\alpha = 2.5$, and (i) $\alpha = 2$.

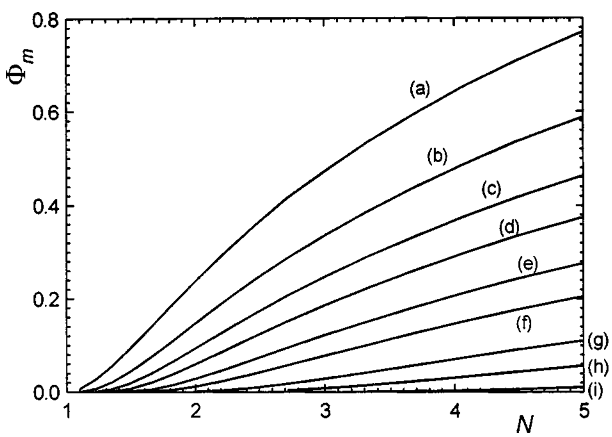

Fig. 8. Same as Fig. 7 except for $\omega_p = \omega_L$.

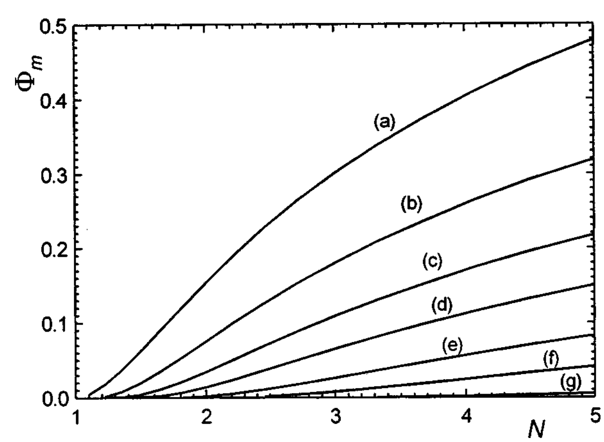

Fig. 9. Same as Fig. 7 except for $\omega_p \ll \omega_L$. Since the Q-switching cannot be realized for $\alpha = 2.5$ and $\alpha = 2$ in the case of both $\omega_p \ll \omega_L$ and $N < 5$, there are no curves (h) and (i) in this figure.

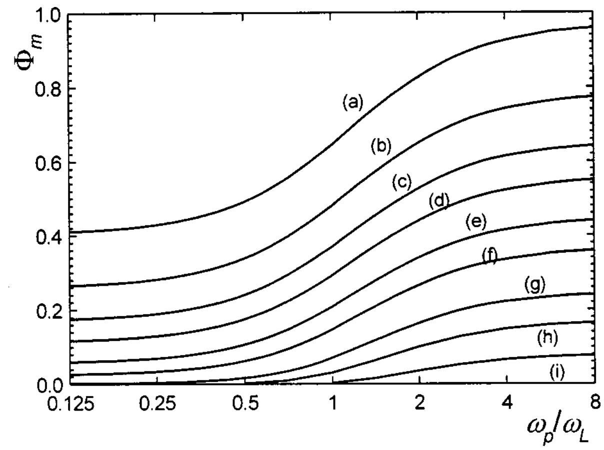

Fig. 10. Relation between Φ_m and ω_p/ω_L for different α in the case of $N = 4$: (a) $\alpha \to \infty$, (b) $\alpha = 20$, (c) $\alpha = 10$, (d) $\alpha = 7$, (e) $\alpha = 5$, (f) $\alpha = 4$, (g) $\alpha = 3$, (h) $\alpha = 2.5$, and (i) $\alpha = 2$.

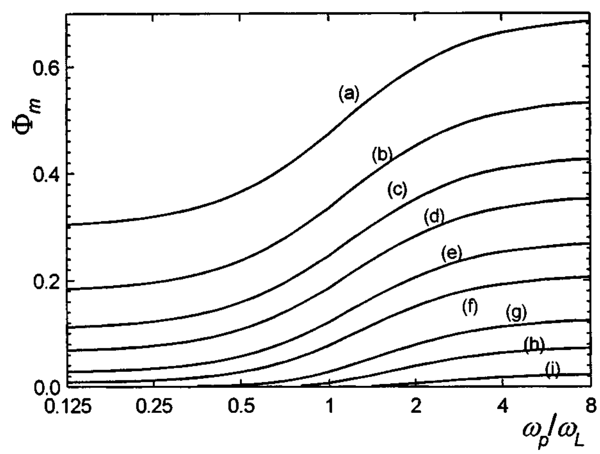

Fig. 11. Same as Fig. 10 except for $N = 3$.

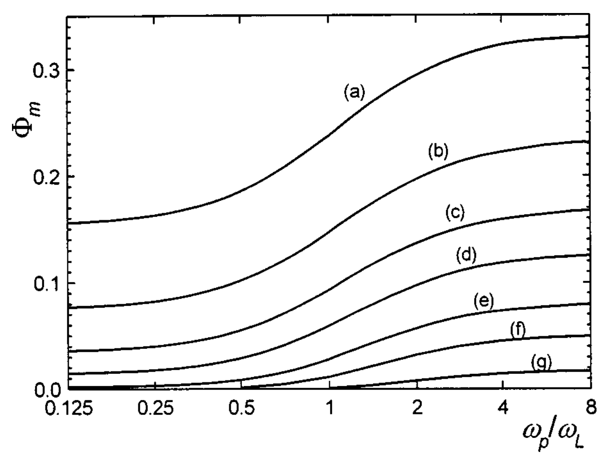

Fig. 12. Same as Fig. 10 except for $N = 2$. Since the Q-switching cannot be realized for $\alpha = 2.5$ and $\alpha = 2$ in the case of both $N = 2$ and $\omega_p/\omega_L < 8$, there are no curves (h) and (i) in this figure.

$\ll \omega_L$, respectively. Figures 16–18 show the variation of $\Delta\tau$ with ω_p/ω_L for different α in the cases of $N = 4$, 3, and 2, respectively. As can be seen from Figs. 13–15, for a given ω_p/ω_L, when α is large, $\Delta\tau$ initially decreases steeply to a minimum value and then increases slightly with increasing N. When α is small, $\Delta\tau$ is large and decreases monotonically with increasing N within the limit of $N < 5$. One can easily understand these results by consulting the results obtained under the plane-wave approximation.[13] As can be seen from Figs. 16–18, for a given N, when α is large, $\Delta\tau$ is small and increases

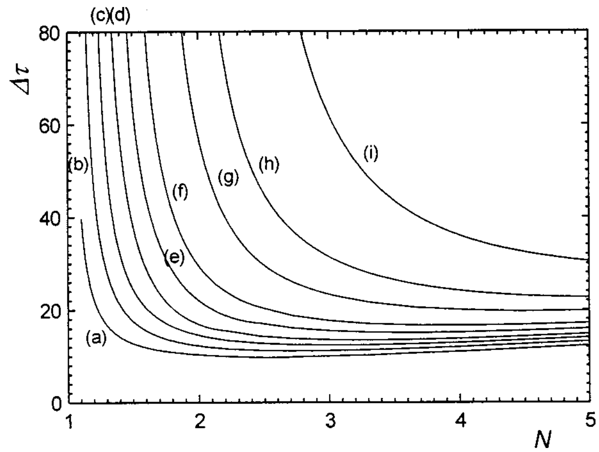

Fig. 13. Relation between $\Delta\tau$ and N for different α in the case of $\omega_p \gg \omega_L$; $\Delta\tau$ is the width (FWHM) of $\Phi(0, \tau)$: (a) $\alpha \to \infty$, (b) $\alpha = 20$, (c) $\alpha = 10$, (d) $\alpha = 7$, (e) $\alpha = 5$, (f) $\alpha = 4$, (g) $\alpha = 3$, (h) $\alpha = 2.5$, and (i) $\alpha = 2$.

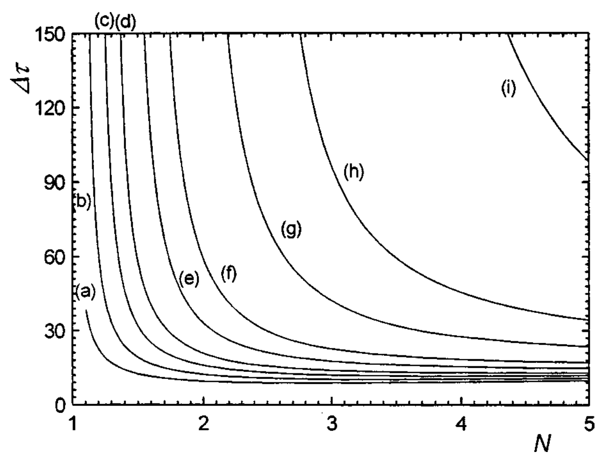

Fig. 14. Same as Fig. 13 except for $\omega_p = \omega_L$.

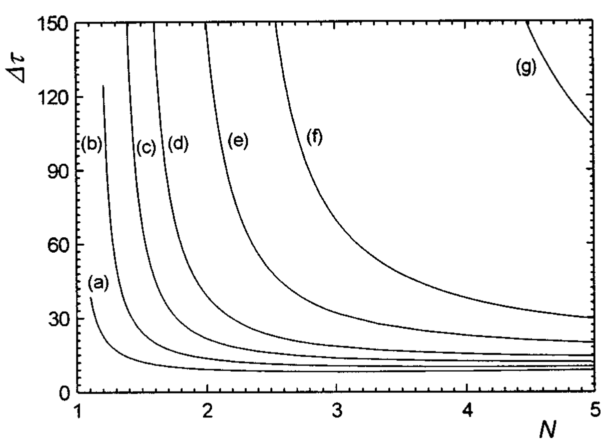

Fig. 15. Same as Fig. 13 except for $\omega_p \ll \omega_L$. Since the Q-switching cannot be realized for $\alpha = 2.5$ and $\alpha = 2$ in the case of both $\omega_p \ll \omega_L$ and $N < 5$, there are no curves (h) and (i) in this figure.

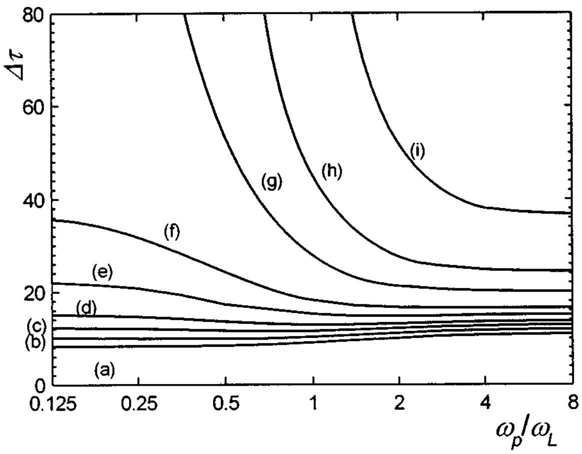

Fig. 16. Relation between $\Delta\tau$ and ω_p/ω_L for different α in the case of $N = 4$: (a) $\alpha \to \infty$, (b) $\alpha = 20$, (c) $\alpha = 10$, (d) $\alpha = 7$, (e) $\alpha = 5$, (f) $\alpha = 4$, (g) $\alpha = 3$, (h) $\alpha = 2.5$, and (i) $\alpha = 2$.

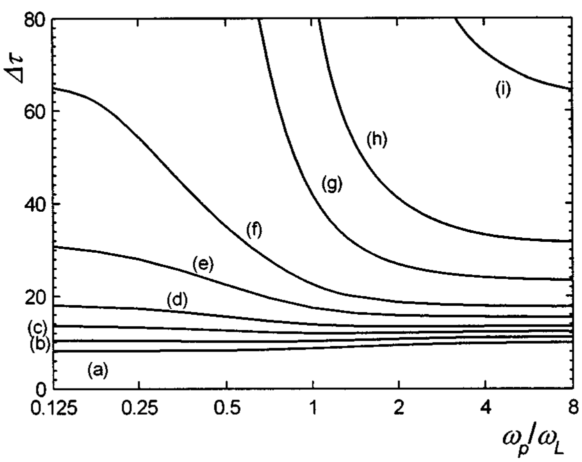

Fig. 17. Same as Fig. 16 except for $N = 3$.

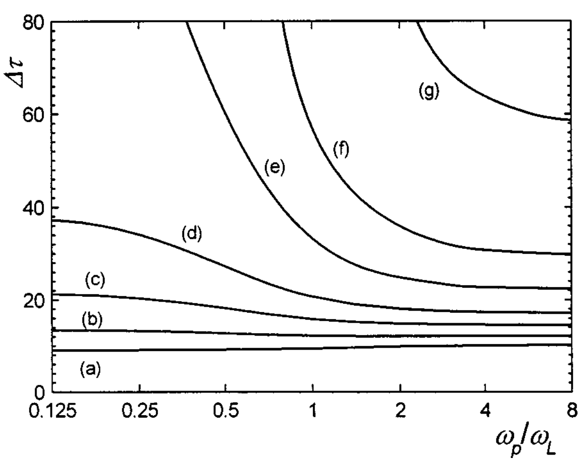

Fig. 18. Same as Fig. 16 except for $N = 2$. Since the Q-switching cannot be realized for $\alpha = 2.5$ and $\alpha = 2$ in the case of both $N = 2$ and $\omega_p/\omega_L < 8$, there are no curves (h) and (i) in this figure.

slightly with increasing ω_p/ω_L. When α is small, $\Delta\tau$ is large and decreases obviously with increasing ω_p/ω_L. The dependence of $\Delta\tau$ on ω_p/ω_L can be understood as follows. When α is large, no matter whether ω_p/ω_L is large or small, the saturable absorber can be easily bleached and the pulse has a small width.[13] When the pulse reaches its peak intensity, only a small part of the inversion population is consumed, there is still quite a lot inversion population that can be consumed and makes the pulse have a longer fall time, and the larger ω_p/ω_L is, the longer the pulse fall time is. This is because, for a large ω_p/ω_L, the peripheral part of the inversion population continues to interact with the laser mode after the central part is depleted. That is to say, the fact that $\Delta\tau$ increases slightly with increasing ω_p/ω_L when α is large is attributed to the normalized pulse fall time increasing slightly with increasing ω_p/ω_L whereas the normalized pulse rise time remains nearly constant.

When α is small, the saturable absorber is not so easy to be bleached, and the pulse has a large width.[13] For a given ω_p, the larger ω_L is, the larger the area in the saturable absorber that needs to be bleached to generate the Q-switched pulse. That is to say, a smaller ω_p/ω_L will make the saturable absorber more difficult to be bleached, and the pulse width will be longer than that obtained in the case of a larger ω_p/ω_L. Therefore $\Delta\tau$ is large and decreases obviously with increasing ω_p/ω_L for a given N and a small α. When α is small, since a larger part of the inversion population has been consumed when the pulse reaches its peak value and only a small part of the inversion population can be used to generate the rear part of the pulse, the pulse fall time is shorter than the rise time.

When α is medium, the situation is between the abovementioned two situations. Now ω_p/ω_L still plays a perceptible role during the bleaching of the saturable absorber. A large ω_p/ω_L is helpful to the bleaching of the saturable absorber, while a small ω_p/ω_L is unfavorable to it. For a medium α and a large ω_p/ω_L the bleaching of the saturable absorber is relatively easy, the pulse width is relatively small and increases very slightly with increasing ω_p/ω_L, and the pulse fall time is slightly longer than the rise time. For a medium α and a small ω_p/ω_L the bleaching of the saturable absorber is relatively difficult, the pulse width is relatively large and decreases obviously with increasing ω_p/ω_L, and the pulse rise time is slightly longer than the fall time.

Sometimes the pulse width W was approximated by the ratio of the pulse energy E to the peak power P_m.[11,13,19,24] So, it is useful to know how much difference exists between W and E/P_m. From Eqs. (23)–(25) it can be seen that the difference between W and E/P_m is directly proportional to that between $\Delta\tau$ and $\Phi_{\text{integ}}/\Phi_m$. In any event, $\Phi_{\text{integ}}/\Phi_m$ is larger than $\Delta\tau$, and the relative error $\varepsilon_r = (\Phi_{\text{integ}}/\Phi_m - \Delta\tau)/\Delta\tau$ depends on α, N, and ω_p/ω_L. But, generally speaking, the larger $\Delta\tau$ is, the larger ε_r is. For example, when $\alpha = 10$ and $N = 4$ and $\omega_p/\omega_L = 1$, $\Delta\tau$ is 11.5 and ε_r is 0.20. When $\alpha = 5$ and $N = 3$ and $\omega_p/\omega_L = 0.5$, $\Delta\tau$ is 22.4 and ε_r is 0.26. When $\alpha = 5$ and $N = 2$ and $\omega_p/\omega_L = 0.5$, $\Delta\tau$ is 60.2 and ε_r is 0.31.

The laser efficiency is also an important parameter. If $\omega_p \ll \omega_L$, nearly all the inversion population can participate in the interaction with the laser mode. If $\omega_p \gg \omega_L$, on the contrary, only the central part of the inversion population can interact with the laser mode; the peripheral part is depleted mainly through spontaneous emission. That is to say, in regard to the ratio of the inversion population participating in the interaction with the laser mode to the total pumped-inversion population,

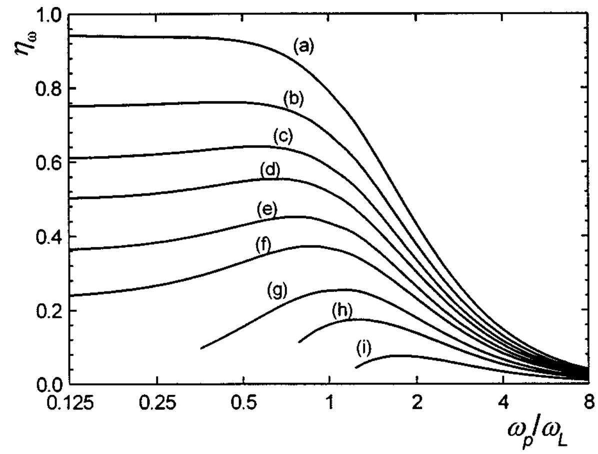

Fig. 19. Relation between η_ω and ω_p/ω_L for different α in the case of $N = 3$: (a) $\alpha \to \infty$, (b) $\alpha = 20$, (c) $\alpha = 10$, (d) $\alpha = 7$, (e) $\alpha = 5$, (f) $\alpha = 4$, (g) $\alpha = 3$, (h) $\alpha = 2.5$, and (i) $\alpha = 2$.

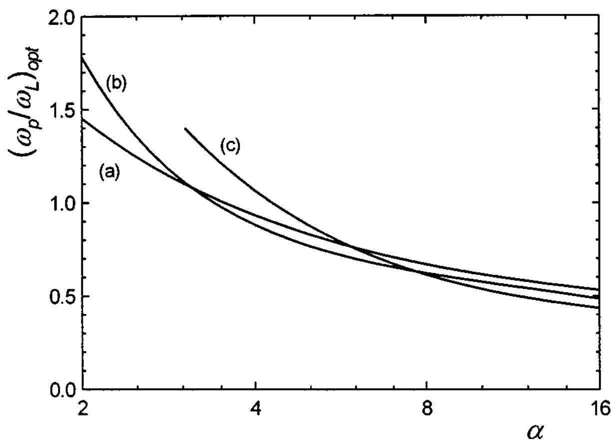

Fig. 20. Relation between $(\omega_p/\omega_L)_{\text{opt}}$ and α for different N: (a) $N = 4$, (b) $N = 3$, and (c) $N = 2$.

a smaller ω_p/ω_L should generate a larger efficiency. On the other hand, for a given ω_p, the larger ω_L is, the larger area in the saturable absorber needs to be bleached to generate the Q-switched pulse, and the larger energy is consumed to bleach the saturable absorber. That is to say, in regard to the bleaching of the saturable absorber, a larger ω_p/ω_L should generate a larger efficiency. Therefore there should be an optimal ω_p/ω_L at which the laser efficiency reaches its maximum value. If the efficiency η is defined as the ratio of the output-pulse energy to the total energy generated when all the initial inversion population is completely depleted by the stimulated emission of the photons, η can be written as

$$\eta = \frac{E}{\dfrac{h\nu}{\gamma}\displaystyle\int_0^\infty\int_0^l n(0,0)\exp\left(-\frac{2r^2}{\omega_p^2}\right)2\pi r\,\mathrm{d}r\,\mathrm{d}z} = \eta_R\eta_\omega, \tag{27}$$

where

$$\eta_R = \frac{\ln\left(\dfrac{1}{R}\right)}{\ln\left(\dfrac{1}{R}\right) + \left(\dfrac{\sigma_{\text{esa}}}{\sigma_{\text{gsa}}}\right)\ln\left(\dfrac{1}{T_0^2}\right) + L}, \tag{28}$$

$$\eta_\omega = \frac{\Phi_{\text{integ}}}{N(1 + \omega_p^2/\omega_L^2)}. \tag{29}$$

η_R is independent of ω_p/ω_L. When the excited-state absorption of the saturable absorber is negligible and $\ln(1/R)$ is much larger than L, η_R approaches unity. Since Φ_{integ} is a function of α, N, and ω_p/ω_L, η_ω is also a function of α, N, and ω_p/ω_L. Figure 19 shows η_ω versus ω_p/ω_L for different α in the case of $N = 3$. In the case of $N = 4$ or 2, the situation is similar. It can be seen that, for each α, there is indeed an optimal ω_p/ω_L, and the larger α is, the smaller the $(\omega_p/\omega_L)_{\text{opt}}$ is. The relation between $(\omega_p/\omega_L)_{\text{opt}}$ and α for different N is shown in Fig. 20.

4. APPLICATIONS

Figures 1–19 can help us understand the dependence of the laser-pulse characteristics on the pump- to laser-mode size ratio and the parameters of the gain medium, the saturable absorber, and the resonator. They can also be used to estimate the pulse parameters. We built a fiber-coupled diode end-pumped passively Q-switched Nd^{3+}:YVO_4 laser using a Cr^{4+}:YAG saturable absorber. The rear face of the gain medium and a plane output coupler constitutes a resonator 3 cm in length, and the flat-flat resonator is stabilized by the thermal lens in the gain medium induced by the pump power. The gain medium length l is 4 mm. The small-signal transmission of the saturable absorber placed near the output coupler T_0 is 79.5%. The reflectivity of the output coupler R is 93.2%. The dissipative loss of the laser L is measured to be 0.03. When the absorbed pump power P_{abs} is 2.2 W, the laser generates a pulse train with a repetition rate of 54 kHz, a pulse energy of 5.0 μJ, a peak power of 0.26 kW, and a pulse width of 19 ns. We treat this laser as an example. The steps for the calculations are as follows. First, determine α, N, and ω_p/ω_L according to Eqs. (20) and (15) and the parameters of the pumping and resonator. For a Nd^{3+}:YVO_4 crystal the effective focal length of the thermal lens induced by the pump power can be approximated by $f = 7.2\omega_p^2/P_{\text{abs}}$, where P_{abs} is in watts, ω_p is in millimeters, and f is in meters.[25] In the case of $\omega_p = 0.41$ mm and $P_{\text{abs}} = 2.2$ W, f is 55 cm. Thus the resonator is equivalent to a plano-concave cavity, and the laser-mode radius ω_L and S_g/S_s are calculated to be 0.211 mm and 1.06, respectively. The other related parameters about the gain medium and saturable absorber are[13,19,24] $\sigma_{\text{gsa}} = 4.3 \times 10^{-18}\,\text{cm}^2$, $\sigma_{\text{esa}} = 8.2 \times 10^{-19}\,\text{cm}^2$, $\sigma = 2.5 \times 10^{-18}\,\text{cm}^2$, and $\gamma = f_a + f_b$, where f_a, f_b are, respectively, the Boltzmann occupation factors of the upper and lower laser levels of the gain medium. For a Nd^{3+}:YVO_4 gain medium at room temperature, $f_a = 0.48$ and $f_b = 0.23$. Thus α, N, and ω_p/ω_L are calculated to be 2.6, 3.0, and 1.9, respectively. Second, we determine Φ_{integ}, Φ_{m}, and $\Delta\tau$ from Figs. 1–18. From Figs. 5, 11, and 17 we obtain $\Phi_{\text{integ}} \approx 2.1$, $\Phi_{\text{m}} \approx 0.04$, and $\Delta\tau \approx 41$. Third, we obtain the pulse energy E, peak power P_m, and pulse width W by using formulas (23)–(25). For this laser, $E = 5.4\,\mu$J, $P_m = 0.25$ kW, and $W = 17$ ns. These theoretical results are in good agreement with the experimental results.

Figures 1–18 are also suitable for flash-lamp-pumped passively Q-switched lasers. For flash-lamp-pumped lasers the initial population-inversion density $n(r, 0)$ can be considered to be uniform, which corresponds to the case of a Gaussian spatial distribution when $\omega_p \to \infty$. Shimony *et al.* have reported a flash-lamp-pumped repetitively Q-switched Nd^{3+}:YAG laser using Cr^{4+}:YAG saturable absorbers.[26] The parameters for this laser are as follows: the cavity length is 82 cm, the gain-medium length l is 104 mm, the output-coupler reflectivity R is 80%, and the initial transmissions of the two Cr^{4+}:YAG saturable absorbers are 81% and 90%, respectively. These data determine the light round-trip transit time $t_r = 6.0\,\text{ns}$ (the refractive index of the gain medium is 1.8). When the saturable absorber with $T_0 = 81\%$ is used, the Q-switched pulse width is 131 ns at low pulse-repetition rate and decreases slightly with the pulse-repetition rate. When the saturable absorber with $T_0 = 90\%$ is used, the pulse width is 277 ns at low pulse-repetition rate and also decreases slightly with the pulse-repetition rate. The pulse energies were not given. We treat this laser at low pulse-repetition rate as an example of flash-lamp-pumped lasers. According to Eq. (20), α is calculated to be 10.9. In calculating α, we use $\sigma_{\text{gsa}} = 4.3 \times 10^{-18}\,\text{cm}^2$, $\sigma_{\text{esa}} = 8.2 \times 10^{-19}\,\text{cm}^2$, $\sigma = 6.5 \times 10^{-19}\,\text{cm}^2$, and $\gamma = f_a + f_b$.[11,13,24] For a Nd^{3+}:YAG gain medium at room temperature, $f_a = 0.41$ and $f_b = 0.19$.[11] Considering that the thermal effect in the gain medium induced by the pump power is not serious at low pulse-repetition rate (i.e., at low pump power), we assume that S_g is equal to S_s. In the case of $T_0 = 81\%$, N is calculated to be 1.97. In calculating N, we use $L = 0.05$. $\Delta\tau$ is obtained to be 14.6 from Fig. 15. The pulse width W is calculated to be 126 ns according to Eq. (23). If L is between 0.03 and 0.08, the theoretical value of the pulse width will be between 125 ns and 127 ns. In the case of $T_0 = 90\%$, then N, $\Delta\tau$, and W are, respectively, 1.54, 22.9, and 284 ns for $L = 0.05$. If L is between 0.03 and 0.08, W will be between 275 ns and 294 ns. These theoretical results are in fair agreement with the experimental results of the pulse width at low pulse-repetition rate. When the pulse-repetition rate is high (i.e., the pump power is high), the smaller pulse width may be attributed to the thermal lens in the gain medium induced by the pump power, which may make S_g larger than S_s, and α becomes larger.

5. CONCLUSIONS

We have numerically solved the space-dependent rate equations of an LD-pumped passively Q-switched laser and generated a group of curves. In the rate equations the intracavity photon density is assumed to be a Gaussian spatial distribution during the entire formatting process of the Q-switched pulse, the population-inversion density at $t = 0$ is also assumed to be a Gaussian spatial distribution [when $t > 0$, $n(r, t)$ can be obtained from Eq. (8)], and the ground-state population density of the saturable absorber at $t = 0$ is assumed to be uniform [when $t > 0$, $n_{\text{sg}}(r, t)$ can be obtained from Eq. (9)]. By normalizing the related parameters, the generated curves are valid for an arbitrary LD-pumped passively Q-switched laser. They are also valid for any passively Q-switched lasers pumped by other lasers and for flash-lamp-pumped passively Q-switched lasers. These curves not only help us have a good understanding of the dependence of the laser-pulse characteristics on the pump- to laser-mode size ratio and the parameters of the gain medium, the saturable absorber, and the resonator, they can also be used to estimate the pulse parameters. Examples have been given to demonstrate the use of the curves and the related formulas.

The dependence of the laser-pulse characteristics on ω_p/ω_L is a major part. The normalized pulse energy and normalized peak power increase monotonically with increasing ω_p/ω_L for given α and N, and the main increments exist in the region near $\omega_p/\omega_L = 1$. When α is small or N is small, the normalized pulse width is large, but decreases steeply with increasing ω_p/ω_L. When α is large, the normalized pulse width is small, but increases slightly with increasing ω_p/ω_L. For given α and N there is an optimal ω_p/ω_L at which the laser efficiency reaches its maximum value; the larger α is, the smaller the $(\omega_p/\omega_L)_{\text{opt}}$ is. Investigations are currently in progress to experimentally measure the variations of pulse parameters with ω_p/ω_L and to compare them with the theoretical results.

ACKNOWLEDGMENTS

This work is partly supported by the National Science Foundation of China, the Science Foundation of Shandong Province, and the Research Fund of Shandong University. Xingyu Zhang gratefully acknowledges the Deutsche Forschungsgemeinschaft. By this financial support, he has the opportunity to conduct cooperative research at the Optical Institute of TU-Berlin. Also he would like to thank Qincheng Zhang for his help in this work.

REFERENCES

1. J. J. Zayhowski and C. Dill III, "Diode-pumped passively Q-switched picosecond microchip lasers," Opt. Lett. **19**, 1427–1429 (1994).
2. P. Wang, Shou-Huan Zhou, K. K. Lee, and Y. C. Chen, "Picosecond laser pulse generation in a monolithic self-Q-switched solid state laser," Opt. Commun. **114**, 439–441 (1995).
3. B. Braun, F. X. Karter, U. Keller, J.-P. Megn, and G. Huber, "Passively Q-switched 180-ps $Nd:LaSc_3(BO_3)_4$ microchip laser," Opt. Lett. **21**, 588–590 (1996).
4. Y. F. Chen, T. M. Huang, and C. L. Wang, "Passively Q-switched diode-pumped $Nd:YVO_4/Cr^{4+}$:YAG single-frequency microchip laser," Electron. Lett. **33**, 1880–1881 (1997).
5. X. Zhang, S. Zhao, Q. Wang, L. Sun, S. Zhang, G. Yao, and Z. Zheng, "Laser diode pumped Cr^{4+}:YAG passively Q-switched Nd^{3+}:S-FAP laser," Opt. Commun. **155**, 55–60 (1998).
6. G. J. Spuhler, R. Paschotta, R. Fluck, B. Braun, M. Moser, G. Zhang, E. Gini, and U. Keller, "Experimentally confirmed design guidelines for passively Q-switched microchip lasers using semiconductor saturable absorbers," J. Opt. Soc. Am. B **16**, 376–388 (1999).
7. A. Szabo and R. A. Stein, "Theory of laser giant pulsing by a saturable absorber," J. Appl. Phys. **36**, 1562–1566 (1965).
8. L. E. Erickson and A. Szabo, "Effect of saturable absorber

lifetime on the performance of giant-pulse lasers," J. Appl. Phys. **37**, 4953–4961 (1966).

9. A. E. Siegman, *Lasers* (University Science, Mill Valley, Calif., 1986), pp. 1024–1026.
10. Y. K. Kuo, M. F. Huang, and M. Birnbaum, "Tunable Cr^{4+}:YSO Q-switched Cr:LiCAF laser," IEEE J. Quantum Electron. **31**, 657–663 (1995).
11. J. J. Degnan, "Optimization of passively Q-switched lasers," IEEE J. Quantum Electron. **31**, 1890–1901 (1995).
12. T. Dascalu, G. Philipps, and H. Weber, "Investigation of a Cr^{4+}:YAG passive Q-switch in CW pumped Nd:YAG laser," Opt. Laser Technol. **29**, 145–149 (1997).
13. X. Zhang, S. Zhao, Q. Wang, Q. Zhang, L. Sun, and S. Zhang, "Optimization of Cr^{4+}-doped saturable-absorber Q-switched lasers," IEEE J. Quantum Electron. **33**, 2286–2294 (1997).
14. L. W. Casperson, "Laser power calculations: sources of error," Appl. Opt. **19**, 422–434 (1980).
15. T. Y. Fan and R. L. Byer, "Diode laser-pumped solid-state lasers," IEEE J. Quantum Electron. **24**, 895–912 (1988).
16. W. P. Risk, "Modeling of longitudinally pumped solid-state lasers exhibiting reabsorption losses," J. Opt. Soc. Am. B **5**, 1412–1423 (1988).
17. Y. F. Chen, C. F. Kao, and S. C. Wang, "Analytical model for the design of fiber-coupled laser-diode end-pumped lasers," Opt. Commun. **133**, 517–524 (1997).
18. Y. F. Chen, T. M. Huang, C. F. Kao, C. L. Wang, and S. C. Wang, "Optimization in scaling fiber-coupled laser-diode end-pumped lasers to higher power: influence of thermal effect," IEEE J. Quantum Electron. **33**, 1424–1429 (1997).
19. X. Zhang, S. Zhao, and Q. Wang, "Modeling of diode-pumped actively Q-switched lasers," IEEE J. Quantum Electron. **35**, 1912–1918 (1999).
20. K. Spariosu, W. Chen, R. Stultz, and M. Birnbaum, "Dual Q-switching and laser action at 1.06 μm and 1.44 μm in a Nd^{3+}:YAG-Cr^{4+}:YAG oscillator at 300 K," Opt. Lett. **18**, 814–816 (1993).
21. M. I. Demchuk, V. P. Milkhailov, N. I. Zhavoronkov, N. V. Kuleshov, P. V. Prokoshin, K. V. Yumashev, M. G. Livshits, and B. I. Minkov, "Chromium-doped forsterite as a solid-state saturable absorber," Opt. Lett. **17**, 929–930 (1992).
22. I. V. Klimov, M. Y. Nikolski, V. B. Tsvetkov, and I. A. Scherbakov, "Passive Q switching of pulsed Nd^{3+} lasers using YSGG:Cr^{4+} crystal switches exhibiting phototropic properties," Sov. J. Quantum Electron. **22**, 603–605 (1992).
23. W. Chen, K. Spariosu, R. Stultz, Y. K. Kuo, M. Birnbaum, and A. V. Shestakov, "Cr^{4+}:GSGG saturable absorber Q switch for the ruby laser," Opt. Commun. **104**, 71–74 (1993).
24. J. J. Degnan, "Theory of the optimally coupled Q-switched laser," IEEE J. Quantum Electron. **25**, 214–220 (1989).
25. Y. F. Chen, C. F. Kao, T. M. Huang, C. L. Wang, L. J. Lee, and S. C. Wang, "Single-mode oscillation of compact fiber-coupled laser-diode-pumped $Nd:YVO_4$/KTP green laser," IEEE Photonics Technol. Lett. **9**, 740–742 (1997).
26. Y. Shimony, Z. Burshtein, A. Ben-Amar Barange, Y. Kalisky, and M. Strauss, "Repetitive Q-switching of a CW Nd:YAG laser using Cr^{4+}:YAG saturable absorber," IEEE J. Quantum Electron. **32**, 305–310 (1996).